**Graduate School of Pure and Applied Sciences**

# Studies on All-Organic Optical Logic Gates by Interconnection of Microresonators

**(マイクロ共振器のインターコネクトによる全有機光ロジックゲートに関する研究)**

Hendra

Doctoral Program in Materials Science
Student ID number: 201930115
Doctor of Philosophy in Engineering
Advised by Professor Yohei Yamamoto

## 1. Introduction

Organic materials have recently received increasing attention in optoelectronics because of their lightweight, high flexibility, compositional diversity, and easy processability. These organic materials are advantageous for realizing flexible optical and optoelectronic devices such as light-emitting diodes, thin-film solar cells, and optical fibers. Particularly, fully organic optical circuits that can be operated entirely by light is highly anticipated for high-speed and long-distance data communication and processing. However, devices so far invented largely rely on inorganic materials and lithographic techniques. For instance, optical logic gates have been realized with optical waveguides in silicon thin wires and optical circuits that combine micro-optical resonators.[15] These optical gates require state-of-the-art advanced microfabrication techniques, which are unapplicable to fully organic devices. An alternative candidate toward this end is an organic microdevice that incorporates photofunctional molecules. Previously, we reported that physically contacted polymer microspheres doped with different organic fluorescent dyes are optically coupled with each other and exhibit cavity-mediated energy transfer. Molecular fluorescence in a sphere is transmitted to the adjacent spheres with a diameter ($d$) of several micrometers, which is far longer than the conventional Förster-type resonant energy transfer process (< 10 nm). Recently, Chandrasekar et al. reported a related work on dye-doped polymer coupled-resonator optical waveguide (CROW), where linearly and L-shaped CROW can transfer light efficiently. However, further functionalization of the spheres, such as a switching operation, rather than the simple light transmission, has not yet been achieved with organic self-assembled microdevices.

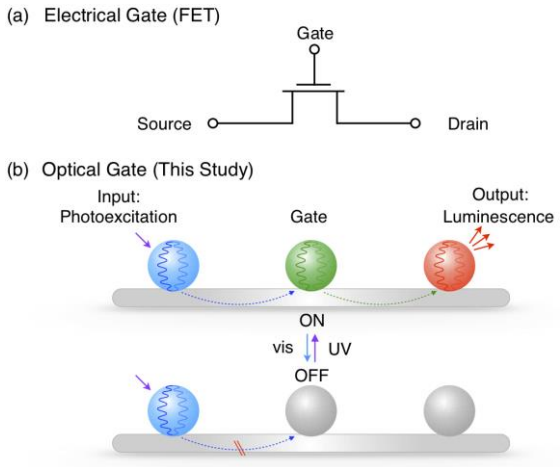


**Figure 1.** Schematic representations of an electronic gate in FET (a) and an optical gate in this study (b). In (b), blue-, green-, and red-emissive polymer microspheres are aligned on an optical microfiber. The green emission from the central microsphere can be switched on and off by UV/visible photoirradiation, leading to the gate operation of the light energy transfer cascade.

In this work, two types of organic material will be employed as host material. In the first work, we used synthetic organic material of polystyrene (PS) to fabricate optical waveguides and microspheres as well. Whereas in the second work, we used natural organic material of spider dragline silk optical fiber and dragline silk protein that converted into the microspheres.

In the first work of my Ph.D., we demonstrate a prototype of a fully organic micro-optical switch consisting of multiple microsphere resonators and an optical fiber. Analogous to an

electric logic gate (Figure 1a), the microspheres individually work as optical source, drain, and gate (Figure 1b). The source sphere, upon optical input, emits fluorescence and illuminates the gate sphere through the optical fiber. The gate sphere, when it is turned on, convert the optical signal to the output sphere. This signal conversion can be switched off by photochemically modulating an organic dye in the gate sphere. All-organic optical switch will be an important step forward to a realization of flexible photonics logic circuits.

In the second work, we demonstrate optical communication in terms of the ratio of the intensity of the integrated device that incorporates SD and recombinant SD silk protein microsphere doped with green-fluorescence dye (N-R6-C) in a micrometer-scale SD optical fiber. The intensity ratio of the optical output to the optical input is analyzed numerically and validated experimentally step by step in the cross-structure, grid-like weave structure of SD, and micrometer-scale of artificial dragline silk. Results show that the average error of numerical analysis again experimental validation in cross-structure, grid-like weave structure (design 1), grid-like weave structure (design 2), and micrometer-scale of artificial spider web are; 5.3%, 6.58%, 10.32%, and 24.21%, respectively, indicating that our model can predict the ratio of intensity within an acceptable range.

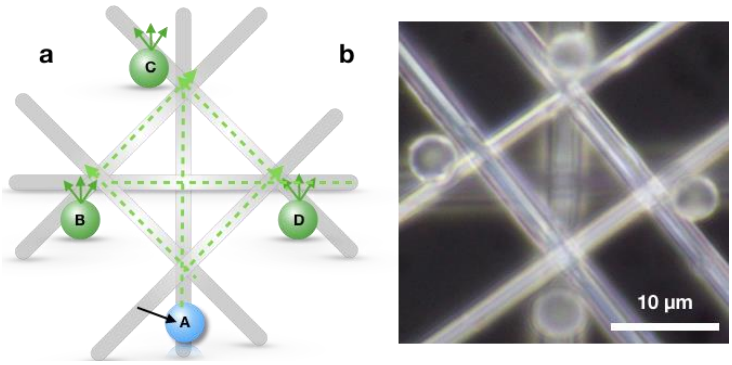


Figure 2. Schematic representation (a) and Optical Microscopy Images (b), of the micrometer-scale Spider web by the Dragline Silk. Using micromanipulation system, the recombinant spider dragline silk protein are immobilized on the micrometer-scale of the artificial spider web.

## 2. Experiments

### 2.1 Preparation Microspheres

In this work, there are two kinds of microsphere that will be used on each part. In the first part, we used the polystyrene (PS) microsphere whereas in the second part, the recombinant spider dragline silk protein will be used.

#### 2.1.1 Preparation of the PS Microspheres

Fluorescent dye-doped PS microspheres were prepared by the interface precipitation method (figure 3). A 200 µL of THF solution containing PS (1 mg) and dye (200 µg) was carefully added onto a water layer (1 mL). Slow diffusion of the solvents takes place along with simultaneous evaporation of THF to give microspheres after overnight.

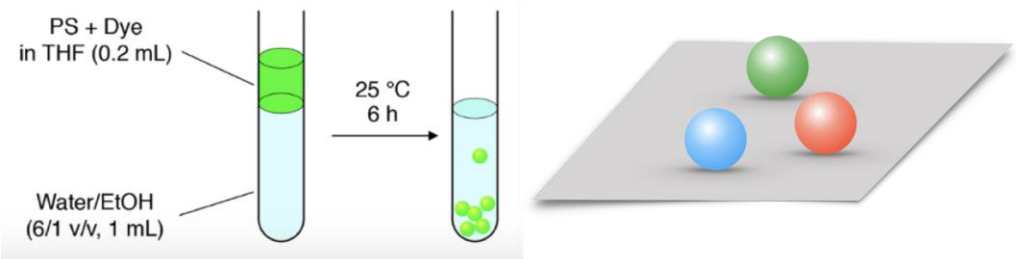


Figure 3. Fabrication of the microsphere by using interface precipitation method

### 2.1.2 Preparation of the recombinant spider dragline protein microsphere

The mixed of 30 µM N-RC-$C^{Dy488}$ with 0.275 M potassium phosphate buffer in pH 7.5 was then thermal ramped from $10^0$C to $60^0$C with the step intervals $10^0$C and 2.5 min/step. After spin down, the pellet was washed in 20 mM of Tris in pH 7.5 along with 0.15 M NaCl. [4

## 2.2 Preparation of the Microfiber

We prepared two kinds of microfiber for each part of the works. In the first part, we used polystyrene (PS) microfiber while in the second part, the spider dragline silk optical fiber will be used as a waveguide.

### 2.2.1 Preparation of the PS microfiber

PS microfibers were prepared by a hand-spinning method (figure 4a). PS polymer was dissolved in dimethylformamide (DMF) with a concentration of 25 wt.%, and the solution was stirred at 25 °C for 24 h with rotation speed at 700 rpm to obtain a homogeneous solution. A small amount of DMF solution was transferred into a thumb. By rapid pressing and pulling away from the solution by thumb and index finger, the uniaxially aligned microfibers were fabricated. To prepare a suspended microfiber, a substrate was gapped by 5 mm distance by using double tape (figure 4b), and uniaxially aligned fiber was transferred in between the gap (figure 4c).

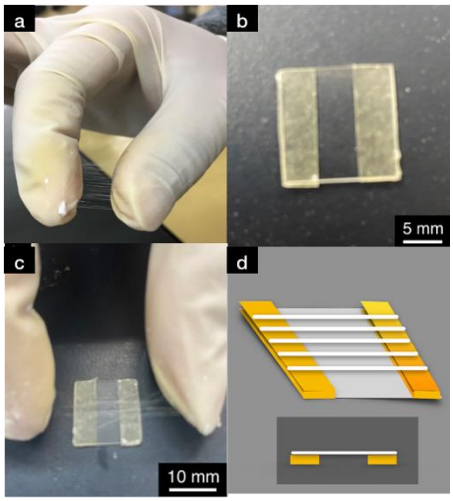


Figure 4. Hand spinning technique a), the gapped substrate b), fiber on the suspended fiber c), and schematic

### 2.2.2 Preparation of the spider dragline silk

The SDS was obtained by reeling the silk directly from the spider.[3] At first, the spider is pinned down after being sedated with carbon dioxide gas. The silk being pulled from the spinnerets consist mainly of the major ampullate silk, which forms the main structure of the web (like scaffolding) and minor ampullate silk, which is used to create the main spiral of the web. The silk thread is pulled over on the spool or bobbin This spider species is possible to harvest between30 – 80 meters of silk in one go.

## 2.3 Mounting of the microsphere on optical fiber

The microspheres were mounted on the suspended fiber as follows [1]: A microsphere with approximately 5 µm in diameter was picked up by using a sharp tip rubber needle equipped on a micromanipulator (MC104 and micro support model Qp-3RH with input AC100-240V 50/60Hz 140 VA, Micro Support, Co, Ltd) on Upright microscope by Olympus model BX53. The microspheres were then transferred onto a selected suspended microfiber. Then, the distance of microspheres was optimized to obtain the desired distance between microspheres (figure 6)


Figure 6. Pickup the microsphere a), transferring the microsphere b), and optimized the distance between the spheres (c).

## 2.4 µ-PL measurements

µ-PL measurements were carried out with a homemade µ-PL measurement system (figure 7). A 405-nm pulsed laser (CNI model MPL-F-355-10 mW-10 %, pulse duration 7 ns, frequency 1 kHz) was passed through ×50 objective lens (NA = 0.9) set on an optical microscope (Nikon model x Eclipse LD100D and exciting a single microsphere (n = 1.59) on quartz substrate (n = 1.47), and PS
microfiber (n = 1.59) . By adjusting the excitation and detection point, luminescence from each microsphere was detected by a spectrometer (Lambda Vision model LV-MC3/T, grating: 300 grooves $mm^{-1}$) through an optical fiber with the spectral resolution of 0.12 nm with 100 µm slit. The schematic representation of the µ-PL setup is drawn in figure 5.

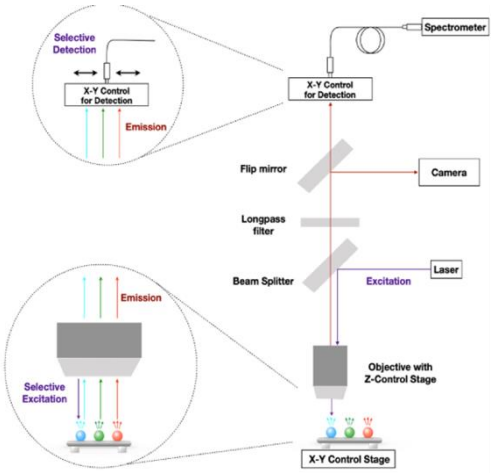


Figure 7. Schematic representation of an experimental setup of µ-PL measurements.

## 3. Results and Discussion

### 3.1 Cavity-Mediated Energy Transfer Cascade and Gate Operation by Photoisomerization

Previously we reported that our group has been successfully investigated the cavity-mediated energy transfer on direct contact of bi-, tri-, and tetra spheres. In this work, we aligned three microspheres of MS-1. MS-$2_{closed}$, and MS-3 in this order on the optical quartz substrate by using a micromanipulation system. Further, we investigate the energy transfer by exciting the source sphere with a 405 nm laser. We observed that the blue, green, and red PL from the MS-1, MS-2, and MS-3 in MS-$2_{closed}$ as shown in figure 4.4, indicating that the energy transfer cascade occurs from MS-1 to MS-$2_{closed}$ and MS-3. The clear WGM was also observed in MS-1, and MS-2 PL spectra indicating that the light confining occurs inside the spheres, while poor WGM observed in PL spectra of MS-3 may be due to the loss of the light confinement. Upon conversion of the MS-2 $_{closed}$ to MS-2 $_{open}$ by irradiation of MS-2 by visible light (400 – 440 nm) for 90 min, resulting in the non-emissive of the MS-2. Upon photoexcitation of the source sphere, only the blue fluorescence that emits from MS-1 is observed, while there is no fluorescence is observed from MS-2 as well as MS-3, indicating that the energy transfer doesn't occur because the light was stopped by non-fluorescence of MS-$2_{open}$ as depicted in figure 8.

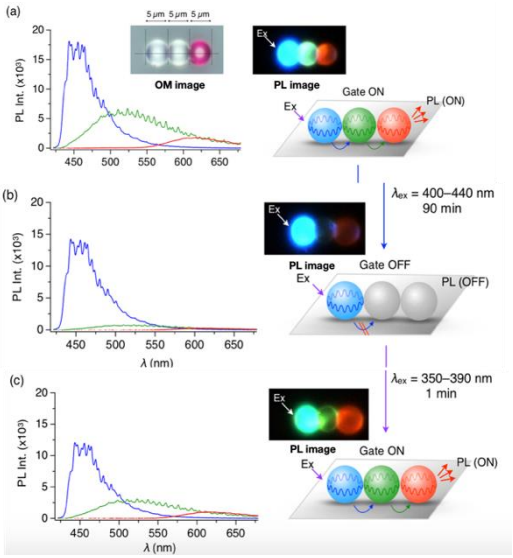


Figure 8 PL spectra, OM and PL image and schematic representation of the trisphere system on the system on the substrate. (a) before photoisomerization, (b) after photoisomerization and (c) after reverse photoisomerization

To further realize the optical logic gate, we irradiate the MS-$2_{open}$ by UV light (350 – 390 nm) for 1 min and it enables to convert from non-fluorescence to re-fluorescence, therefore its convert of MS-$2_{open}$ to MS-$2_{closed}$. Upon photoexcitation of the source sphere, the blue, green, and red fluorescence are observed from MS-1, MS-2closed, and MS-3.

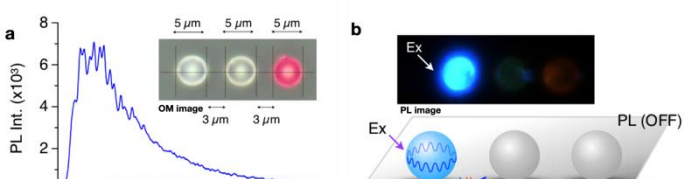


Figure 9. PL spectra from MS-1, MS-$2_{closed,}$ and MS-3 (a), upon photoexcitation of the MS-1, only blue fluorescence is observed from MS-1, while there is no fluorescence is observed from MS-$2_{closed}$, and MS-3 ($b_{top}$)

We also investigate that physically non-contact of the sphere, the energy transfer hardly occurs (figure 9). We arrange the MS-1, MS-2closed, and MS-3 on the optical quartz substrate with the distance of about 3 μm from each other. Upon photoexcitation of the blue sphere as an input source, only the blue fluorescence is observed from MS-1 while there is no fluorescence is observed from MS-$2_{closed}$ as well as MS-3.

### 3.2 Arranging Microspheres on Suspended Polymer Fiber for Long-Distance Light Transportation

To investigate the long-distance light transportation, at first, we prepared two microsphere MS-**1** and MS-**2** with the diameter *d* of about 5 μm were carefully transferred onto suspended microfiber with the distance of each other of about 2.5 μm (Figure 4.6a inset). Upon photoexcitation on the MS-**1**, the blue and green fluorescence are observed from MS-1 and MS-2 (Figure 4.6a right), indicating that the energy is transferred from MS-1 to MS-2 through the optical fiber with clear WGM (Figure 4.6a left). Further, when the MS-$2_{closed}$ and MS-3 were mounted on the suspended microfiber, at the distance *d* of about 2.5 μm, upon photoexcitation on the MS-2, the green fluorescence and red fluorescence are observed indicating that energy transfer occurs from the green sphere to the red sphere trough the optical fiber with clear WGM.

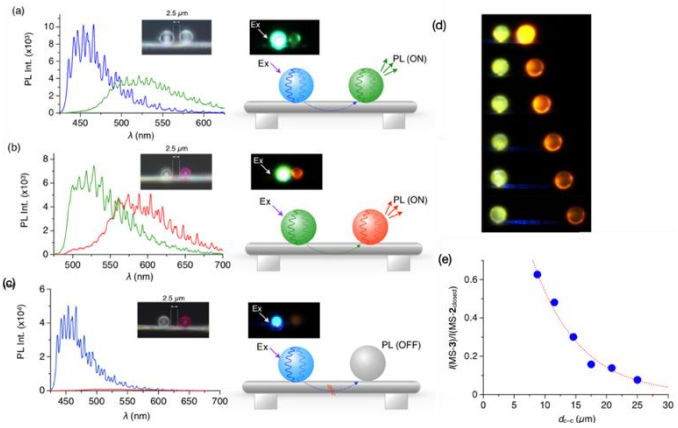


Figure 10 (a–c) Right: Schematic illustrations of two microspheres (a MS-**1** and MS-$\mathbf{2}_{closed}$; b, MS-$\mathbf{2}_{closed}$ and MS-**3**; c, MS-**1** and MS-**3**, *d* of each sphere: 5 μm), which are mounted on a suspended fiber with 2.5 μm separation. Left: PL spectra from a single microsphere upon focused laser excitation of the microsphere on the left side. Insets show OM images. (d) FM images of MS-$\mathbf{2}_{closed}$ and MS-**3** (*d* of each sphere: 5 μm) mounted on a suspended fiber, upon laser excitation of MS-$\mathbf{2}_{closed}$. (e) Plot of ($I$(MS-**3**)/$I$(MS-$\mathbf{2}_{closed}$)) versus $d_{c\text{-}c}$. The red curve indicates exponential fitting by equation (2) with $A$ = 2.01 and $R$ = 0.13.

On the other hand, as predicted from the small spectral overlaps between the emission of the blue and absorption of the red, when the MS-1 and MS-3 are mounted on the suspended microfiber, upon photoexcitation of the MS-1, only blue fluorescence is observed, while there is no fluorescence being observed from MS-3, indicating the energy transfer is hardly occur from MS-1 to MS-3. (Figure 10 c right). Distance dependent of the light transmission is investigated using MS-$2_{closed}$ and MS-3 on the suspended microfiber. By increasing the distance between MS-$2_{closed}$ and MS-3 on the suspended microfiber, upon laser excitation on the MS-$2_{closed}$, the PL intensity of MS-3 was decreased (Figure 10 d). A plot of the ratio of the intensity of MS-3 to MS-$2_{closed}$ ($I$(MS-3)/$I$(MS-$2_{closed}$)) versus $d_{c\text{-}c}$ shows an exponential decay (Figure 10e. We evaluated the distance-dependent of energy transfer efficiency of about 0.13 using the following equation;

$$(I(\text{MS-3})/I(\text{MS-2}_{closed})) = A\exp(-Rdc\text{-}c) \qquad (1)$$

### 3.3 Optical Gate Operation from Three and tetra Spheres

For optical gate operation (Figure 11a), MS-1, MS-$2_{closed}$, and MS-3 are mounted on the suspended fiber in this order with a separation of 2.5 μm (Figure 11b inset, top). Upon focused laser excitation of MS-1, PLs from all the spheres are observed (Figure 11b inset, bottom), indicating the PL transfer cascade occurs from MS-1 to MS-$2_{closed}$ through the optical fiber and subsequently from MS-$2_{closed}$ to MS-3 (Figure 9$b_{left}$). PL spectra from each microsphere involve WGMs, indicating that the generated PL is confined in each microsphere.

Optical gate operation experiments are then carried out by photoexcitation of MS-2 with 400–440 nm light, leading to photochemical isomerization from $2_{closed}$ to $2_{open}$ (Figure 11b and c right). Upon focused laser excitation to MS-1, PL from MS-3 is very weak (Figure 11c inset). As shown in Figure

11c $_{left}$, PL spectra from MS-2$_{open}$ and MS-3 display very small PL intensity, showing the successful gate operation to switch off the cascade of the light transportation. Furthermore, once 2$_{open}$ turns back to 2 $_{closed}$ by photoirradiation with 350–390 nm light, red-color PL from MS-3 recovers upon laser excitation of MS-1 (Figure 11d)

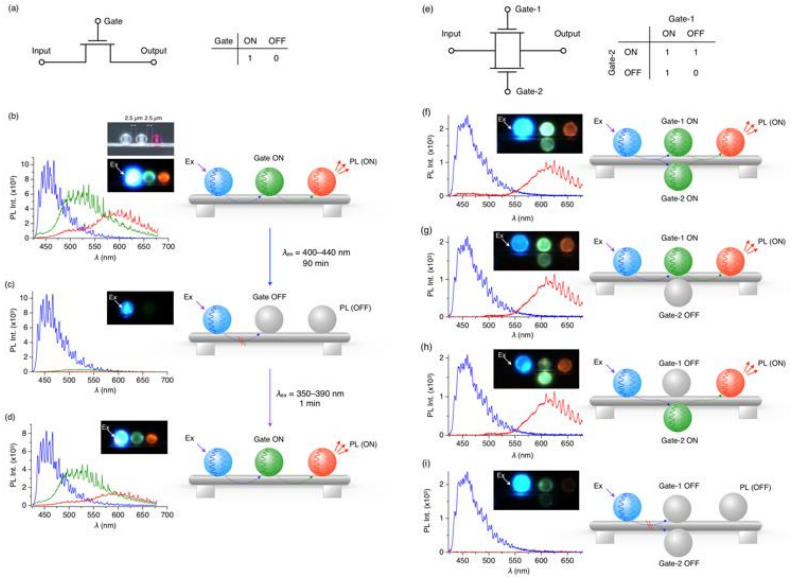

**Figure 11.** Schematic representation of three (a) and four (e) terminal gate, optical logic gate on three spheres before photoisomerization (b), after photoisomerization (c), and after reverse photoisomerization (d). Optical logic gate on tetra sphere, gate 1 and 2 are closed state (f), gate 1 is closed state (g), gate 2 is closed state (h), and gate 1 and 2 are open state (i)

Based on the PL intensity ratio and Q-factor, the efficiency of the PL transfer and resonator property of the directly contacted and separated microspheres on a fiber are discussed. The ratio of the light energy transfer, *r*, between microspheres is defined as PL intensity ratio from one sphere to the other, described as follows:

$$r_{1\text{-}2} = I(\text{MS-}\mathbf{2}_{\text{closed}})/I(\text{MS-}\mathbf{1}) \quad (2)$$

$$r_{2\text{-}3} = I(\text{MS-}\mathbf{3})/I(\text{MS-}\mathbf{2}_{\text{closed}}) \quad (3)$$

For directly contacted trisphere on a fiber (Figure 12), the $r_{1\text{-}2}$ and $r_{2\text{-}3}$ values are evaluated as 0.83 and 0.67, respectively. On the other hand, for 2.5-μm-separated three spheres on an optical fiber, the $r_{1\text{-}2}$ and $r_{2\text{-}3}$ values are 0.69 and 0.55, respectively, which are ~0.8 times smaller than the directly connected trisphere. Meanwhile, Q-factors, defined as the WGM peak wavelength divided by the full width at half-maximum of the peak, for MS-**1**, MS-**2**$_{closed}$, and MS-**3**, separated with one another by 2.5 μm on a PS fiber, are 170, 380, and 410, upon excitation of MS-**1**. These values are higher than those for directly contacted MS-**1**, MS-**2**$_{closed}$, and MS-**3** on a fiber (130, 190, and 320, respectively). These differences are possibly caused by the difference of the number of the contact points that causes an optical loss for the resonator, and the separated microspheres on a fiber are advantageous for preserving high resonator properties.

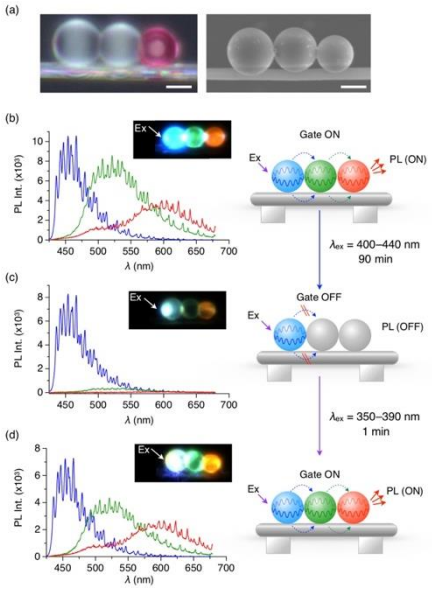

Figure 12. Optical logic gate operation on direct contact of trisphere system on the fiber

We further investigate optical gate operation to realize OR logic gate using four microspheres (Figure 11f). As schematically drawn in Figure 11f–i, two optical gates (MS-**2**) are located in parallel between MS-**1** and MS-**3** on the optical fiber, and ON/OFF gate operations are carried out by photoisomerization of

**2** upon shining focused UV or visible laser onto each of MS-**2**. The optical output (PL from MS-**3**) turns ON upon excitation of MS-**1** when either of gate-1 or gate-2 are ON (Figure 11f–h), meanwhile, the optical output turns OFF when both of MS-**2 is** in the OFF state (Figure 11i).

### 3.4 Coefficient optical loss of spider dragline optical fiber

We measured an optical loss coefficient and exponential decay of the optical loss spider dragline silk by distance dependency method as described on figure 4.6. We plotted the value of the ratio of intensity again their center-to-center distance to determine the optical loss coefficient by determining the exponential decay equation (figure 5.6h). It was found that the coefficient optical loss of about 0.03 dB/µm and ratio of intensity was exponentially decayed following the equation as follow;

$$Y = 1.0631e^{-(0.03).d(c-c)} \qquad (4)$$

### 3.5 Prediction model of energy transfer efficiency

In this part, we calculate the energy transfer efficiency in terms of the ratio of intensity between optical output and optical input in cross-structure, grid-like weave structure, and micrometer-scale of an artificial spider web.

### 3.5.1 Prediction model of energy transfer efficiency in cross-structure

Energy transfer efficiency is defined as the ratio of intensity between the highest peak of optical output luminescence and the highest peak of the optical input photoexcitation. The energy transfer efficiency is calculated. In this part, the energy transfer efficiency of the interconnected microresonator on the cross-structure is calculated. Further, an energy transfer efficiency prediction model on the complex structure such as grid-like weave structure and micrometer-scale of the artificial spider web which contains multiple junctions rather than cross-structure will be generated. On each structure, we believe that the light will be transferred fiber to fiber and fiber to the sphere. By considering the Snell law, the light will be transferred efficiently when the refractive index between two mediums is not so large.

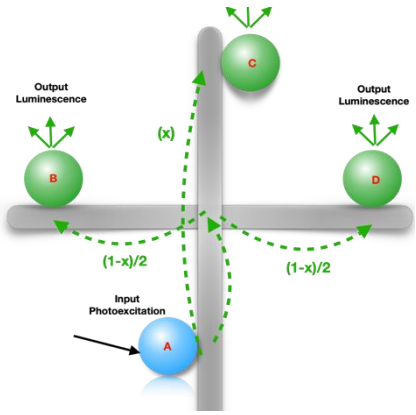


Figure 13. Schematic representation of the incorporation of the microresonator interconnected with the SDS

In this study, we demonstrated the fiber-sphere coupled in case of cross-structure and grid-like weave structure, whereas fiber-fiber-sphere coupled in case of micrometer-scale of the artificial spider web structure.

We obtained the numerical calculation equation to predict the energy transfer efficiency between optical output and optical input in cross-structure as follows;

$$I_{MSb/MSa} = (1-x)/2.(1.0631e^{(-0.03)d_{a-b}}) \qquad (5)$$

$$I_{MSc/MSa} = x.(1.0631e^{(-0.03)d_{a-c}}) \qquad (6)$$

$$I_{MSb/MSa} = (1-x)/2.(1.0631e^{(-0.03)d_{a-b}}) \qquad (7)$$

The numerical result of the energy transfer efficiency in terms of ratio of intensity of $I_{MSb/MSa}$, and $I_{MSd/MSa}$ are 0.1854 and 0.1910 respectively while $I_{MSc/MSa}$ is 0.3508

### 3.5.1 Prediction model of energy transfer efficiency in the grid-like weave structure

We extent the cross-structure which has a single junction to a more complex structure such as a grid-like weave structure that has multiple junctions to predict the energy transfer efficiency of the source sphere again the output spheres. In this structure, the light from the source will be passed through several junctions before reaching the output sphere. In this work, the output microresonator spheres will be placed on vertical SDS and horizontal SDS as depicted in figure 14.

We obtained that the numerical calculation of the ratio of intensity in grid-like weave structure for design 1 is; 0.1562, 0.0297, and 0.0420, for $I_{b/a,}$ $I_{c/a}$, and $I_{d/a}$ while in design 2 is 0.1863, 0.0709, 0.0373, and 0.0761 for $I_{b/a,}$ $I_{c/a}$, $I_{d/a,}$ and $I_{e/a,}$ respectively

### 3.5.2 Prediction model of energy transfer efficiency in micrometer-scale of spider web

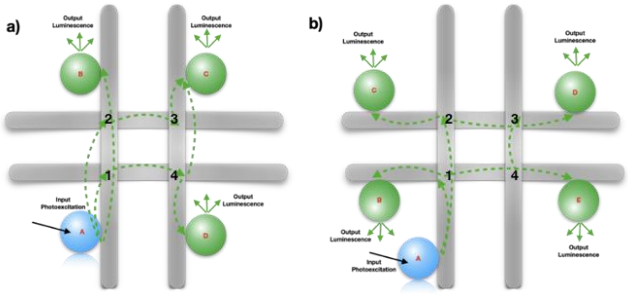


Figure 14 Schematic representation of the incorporation of microresonator interconnected by grid-like weave structure of SDS. a) Microresonators were placed on two pieces of vertical SDS, b) microresonators were

We generate the formula to determine the intensity ratio between the optical output and optical input. Upon photoexcitation of the input sphere, the light will be propagated along the SDSs and illuminate all output spheres. The light will be passed through several junctions at different pathways to reach the particular output sphere. We obtained the numerical calculation of the ratio of intensity for $I_{b/a,}$ $I_{c/a}$, and $I_{d/a}$ in micrometer-scale of the spider web is 0.0761, 0.099, and 0.074 respectively.

### 3.5.3 Experimental result of energy transfer efficiency in cross-structure, grid-like weave design 1 and 2, and in micrometer-scale of artificial spider web

We summarized the results of the numerical analysis and experimental validation of the ratio of the intensity between the optical output and optical input in cross-structure, grid-like weave structure, and micrometer-scale of the artificial spider web structure as shown in figure 15, and we also calculate the percentage of error, to measure how precise our calculation again experimental results as shown in figure 16. The percentage of error in the numerical calculation versus experimental validation in cross-structure show an average of about 5.3%, whereas in the grid-like weave structure design 1 and 2, the average of errors of about 6.6% and 10.3%. The percentage of error in micrometer-scale artificial spider web structure shows an average of about 24.2%. The results indicate that our model can predict the ratio of intensity within an acceptable range.

Table 1 Numerical and experimental calculation of the ratio of the intensities of the optical output and optical input in cross-structure, grid-like weave structure design 1, and grid-like weave structure design 2 and micrometer-scale of the artificial spider web

| **Structure Design** | **Method** | $I_{B/A}$ | $I_{C/A}$ | $I_{D/A}$ | $I_{E/A}$ |
|---|---|---|---|---|---|
| Cross-structure | Numerical | 0.1854 | 0.3508 | 0.1910 | - |
| | Experimental | 0.1671 | 0.3508 | 0.1896 | - |
| Grid-like weave Design 1 | Numerical | 0.1562 | 0.0297 | 0.0420 | |
| | Experimental | 0.1566 | 0.0333 | 0.0389 | |
| Grid-like weave Design 2 | Numerical | 0.1863 | 0.0709 | 0.0373 | 0.0761 |
| | Experimental | 0.1979 | 0.0826 | 0.0389 | 0.087 |
| Micrometer-scale of the artificial spider web | Numerical | 0.0761 | 0.099 | 0.074 | |
| | Experimental | 0.04809 | 0.0835 | 0.0583 | |

Table 2 Percentages of Error the Numerical Analysis Again Experimental validation

| **Structure Design** | $I_{B/A}$ *(%)* | $I_{C/A}$ *(%)* | $I_{D/A}$ *(%)* | $I_{E/A}$ *(%)* | ***Average*** |
|---|---|---|---|---|---|
| Cross-structure | 9.87 | - | 0.73 | | 5.3 |
| Grid-like weave Design 1 | 0.25 | 12.12 | 7.38 | | 6.8 |
| Grid-like weave Design 2 | 6.21 | 16.50 | 4.28 | 14.32 | 10.32 |
| Micrometer-scale of the artificial spider web | 35.74 % | 15.65 % | 21.21 % | | 24.2 |

**References**


[1] Y. Shirota, *J. Mater. Chem.* **2000**, *10*, 1.
[2] F. S. Kim, G. Ren, S. A. Jenekhe, *Chem. Mater.* **2011**, *23*, 682.
[3] R. Chandrasekar, *Phys. Chem. Chem. Phys.* **2014**, *16*, 7173.
[4] G. C. Righini, J. Krzak, A. Lukowiak, G. Macrelli, S. Varas, M. Ferrari, *Opt. Mater. (Amst).* **2021**, *115*, 111011.
[5] L. Zhang, B. Li, B. Lei, Z. Hong, W. Li, *J. Lumin.* **2008**, *128*, 67.
[6] I. Song, J. Ahn, X. Shang, J. H. Oh, *ACS Appl. Mater. Interfaces* **2020**.
[7] F. Castet, V. Rodriguez, J. L. Pozzo, L. Ducasse, A. Plaquet, B. Champagne, *Acc. Chem. Res.* **2013**, *46*, 2656.
[8] G. Zhao, H. Dong, Q. Liao, J. Jiang, Y. Luo, H. Fu, W. Hu, *Nat. Commun.* **2018**, *9*.
[9] C. Zhang, C. L. Zou, Y. Zhao, C. H. Dong, C. Wei, H. Wang, Y. Liu, G. C. Guo, J. Yao, Y. S. Zhao, *Sci. Adv.* **2015**, *1*:e1500257.
[10] T. Amemiya, T. Kanazawa, T. Hiratani, D. Inoue, Z. Gu, S. Yamasaki, T. Urakami, S. Arai, *Opt. Express* **2017**, *25*, 18537.
[11] S. Kita, K. Nozaki, K. Takata, A. Shinya, M. Notomi, *Commun. Phys.* **2020**, *3*:33.
[12] A. Fushimi, T. Tanabe, *Opt. Express* **2014**, *22*, 4466.
[13] D. Okada, T. Nakamura, D. Braam, T. D. Dao, S. Ishii, T. Nagao, A. Lorke, T. Nabeshima, Y. Yamamoto, *ACS Nano* **2016**, *10*, 7058.
[14] O. Oki, S. Kushida, A. Mikosch, K. Hatanaka, Y. Takeda, S. Minakata, J. Kuwabara, T. Kanbara, T. D. Dao, S. Ishii, T. Nagao, A. J. C. Kuehne, F. Deschler, R. H. Friend, Y. Yamamoto, *Mater. Chem. Front.* **2018**, *2*, 270.
[15] S. Lee, J. Lee, S. Hohng, *PLoS One* **2010**, *5*, e12270.
[16] D. Kim, T. Lee, Y.-S. Lee, T. Watanabe, *Curr. Appl. Phys.* **2018**, *18*, S14.
[17] D. Okada, Z. H. Lin, J. S. Huang, O. Oki, M. Morimoto, X. Liu, T. Minari, S. Ishii, T. Nagao, M. Irie, Y. Yamamoto, *Mater. Horizons* **2020**, *7*, 1801.
[18] M. Irie, M. Morimoto, *Bull. Chem. Soc. Jpn.* **2018**, *91*, 237.
[19] S. Kushida, D. Braam, C. Pan, T. D. Dao, K. Tabata, K. Sugiyasu, M. Takeuchi, S. Ishii, T. Nagao, A. Lorke, Y. Yamamoto, *Macromolecules* **2015**, *48*, 3928.
[20] K. Tabata, D. Braam, S. Kushida, L. Tong, J. Kuwabara, T. Kanbara, A. Beckel, A. Lorke, Y. Yamamoto, *Sci. Rep.* **2014**, *4*, 5902.
[21] D. Braam, S. Kushida, R. Niemöller, G. M. Prinz, H. Saito, T. Kanbara, J. Kuwabara, Y. Yamamoto, A. Lorke, *Sci. Rep.* **2016**, *6*, 19635.
[22] M. Kuwata-Gonokami, S. Ozawa, R. H. Jordan, A. Dodabalapur, H. E. Katz, M. L. Schilling, R. E. Slusher, *Opt. Lett.* **1995**, *20*, 2093.
[23] A. V Veluthandath, P. B. Bisht, *J. Lumin.* **2017**, *187*, 255.
[24] S. Kushida, D. Braam, T. D. Dao, H. Saito, K. Shibasaki, S. Ishii, T. Nagao, A. Saeki, J. Kuwabara, T. Kanbara, M. Kijima, A. Lorke, Y. Yamamoto, *ACS Nano* **2016**, *10*, 5543.
[25] K. Watanabe, B. S. Kim, Y. Enomoto, I. S. Kim, *Macromol. Mater. Eng.* **2011**, *296*, 568.
[26] J. Zhao, T. Zhang, X. Y. Dong, M. E. Sun, C. Zhang, X. Li, Y. S. Zhao, S. Q. Zang, *J. Am. Chem. Soc.* **2019**, *141*, 15755.
[27] Y. Takagi, M. Morimoto, R. Kashihara, S. Fujinami, S. Ito, H. Miyasaka, M. Irie, *Tetrahedron* **2017**, 4918